

Highly Efficient Wave-Front Reshaping of Surface Waves with Dielectric Metawalls

Shaohua Dong,^{1,2} Yu Zhang,³ Huijie Guo,³ Jingwen Duan,^{1,2} Fuxin Guan,³
Qiong He,^{3,4} Haibin Zhao,¹ Lei Zhou,^{3,4} and Shulin Sun^{1,2,*}

¹*Shanghai Engineering Research Center of Ultra-Precision Optical Manufacturing, Green Photonics and Department of Optical Science and Engineering, Fudan University, Shanghai 200433, China*

²*State Key Laboratory of Applied Optics, Changchun Institute of Optics, Fine Mechanics and Physics, Chinese Academy of Sciences, Changchun 130033, China*

³*State Key Laboratory of Surface Physics and Key Laboratory of Micro and Nano Photonic Structures (Ministry of Education), Fudan University, Shanghai 200433, China*

⁴*Collaborative Innovation Center of Advanced Microstructures, Nanjing 210093, China*



(Received 24 October 2017; published 30 January 2018)

Controlling the wave fronts of surface waves (including surface-plamon polaritons and their equivalent counterparts) at will is highly important in photonics research, but the available mechanisms suffer from the issues of low efficiency, bulky size, and/or limited functionalities. Inspired by recent studies of metasurfaces that can freely control the wave fronts of propagating waves, we propose to use metawalls placed on a plasmonic surface to efficiently reshape the wave fronts of incident surface waves (SWs). Here, the metawall is constructed by specifically designed meta-atoms that can reflect SWs with desired phases and nearly unit amplitudes. As a proof of concept, we design and fabricate a metawall in the microwave regime (around 12 GHz) that can anomalously reflect the SWs following the generalized Snell's law with high efficiency (approximately 70%). Our results, in excellent agreement with full-wave simulations, provide an alternative yet efficient way to control the wave fronts of SWs in different frequency domains. We finally employ full-wave simulations to demonstrate a surface-plasmon-polariton focusing effect at telecom wavelength based on our scheme.

DOI: 10.1103/PhysRevApplied.9.014032

I. INTRODUCTION

Surface waves (SWs), including surface-plasmon polaritons (SPPs) and their equivalent counterparts such as spoof SPPs and guided SWs, have attracted considerable interest in photonic research [1]. Two extraordinary properties, subwavelength resolution and local field enhancement, offered SWs many applications in practice, such as super-imaging [2,3], biological and chemical sensing [4], and on-chip photonic circuits [5]. Obviously, efficiently controlling the wave fronts of SWs is the basis to realize these applications. Some micro-optical elements, e.g., cylindrical or triangular dielectric disks, are utilized to refract or focus SWs [6,7]. However, these conventional devices to control SW wave fronts typically exhibit large sizes and/or limited functionalities.

With the development of nanophotonics, many new schemes were proposed to control the SW wave fronts, yielding fascinating effects such as SW deflection [8–10], Airy-beam generation [11,12], SW focusing [13–15], and holograms [16,17]. These devices typically consist of grooves, holes, and slits patterned on a flat plasmonic

metal, relying on Bragg scatterings for wave-front controls. Meanwhile, gradient metamaterials were also designed to achieve the cloaking effect for SWs based on the transformation-optics theory [18–20]. Although these schemes have shown great potential to control SW wave fronts, the size of these devices is relatively large (in terms of SW wavelength) or the working efficiency is low, and, thus, they are unfavorable for highly integrated on-chip photonic applications.

Along a parallel line, metasurfaces [ultrathin metamaterial layers constructed by planar meta-atoms with pre-determined electromagnetic wave (EM) properties] have significantly expanded our capabilities to control the wave fronts of free-space light. Designing metasurfaces with the appropriate reflection or transmission and amplitude or phase distributions, one can control the wave fronts of light incident on the metasurfaces based on Huygens' principle, leading to various fascinating wave-manipulation effects such as anomalous transmission or reflection [21–23], conversion from propagating waves (PWs) to SWs [24–28], flat-lens focusing [29–32], complex beam generation [33–35], holographic imaging [36–38], amplitude- and phase-controlled SW excitation [39], two-dimensional light control with light [40], and beam splitters [41]. Such a scheme has the advantages of highly compact device size and

*Corresponding author.
sls@fudan.edu.cn

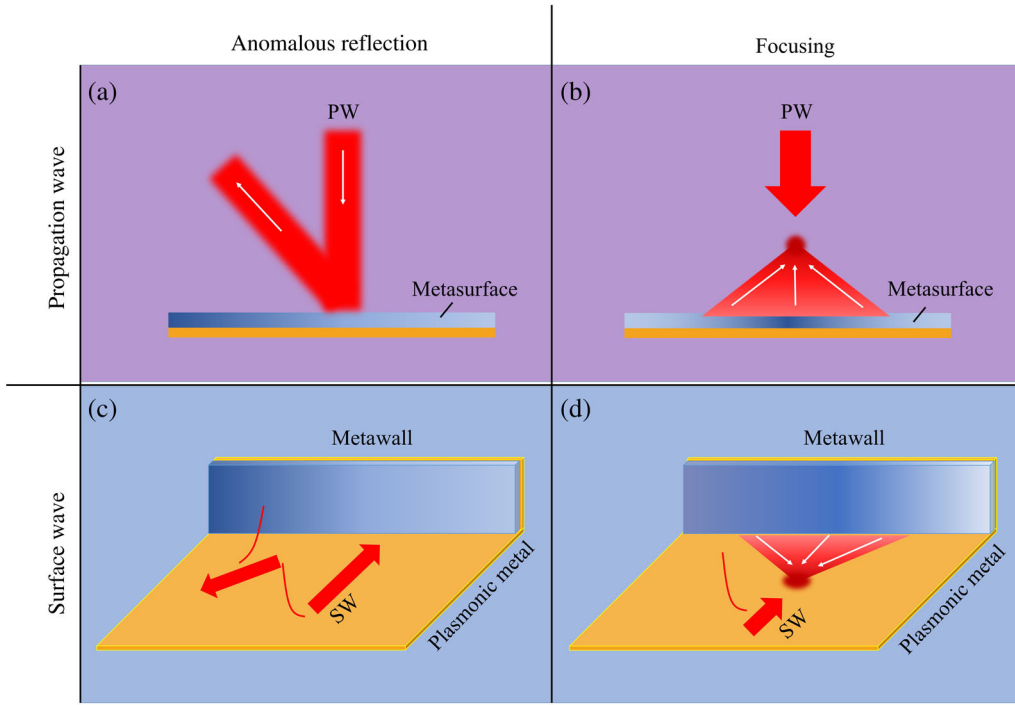


FIG. 1. Concept of wave-front modulations with gradient metasurfaces for propagating waves and surface waves. A metasurface exhibiting a (a) linear or (b) parabolic reflection phase distribution can realize anomalous reflection (a) and focusing effects (b) for propagation waves. A metawall exhibiting a (a) linear or (b) parabolic reflection phase distribution can realize anomalous reflection (a) and focusing effects (b) for the SW.

high working efficiency, both being highly desired in integrated-photonics applications. However, so far, most work based on such a scheme is on controlling PWs instead of SPPs.

In this work, we extend the concept of metasurfaces to the field of SW manipulations. We first show that an ultrathin dielectric and metal structure placed vertically on a plasmonic metal can efficiently reflect SWs with the phase dictated by the permittivity of the dielectric layer. This motivates us to build a metawall using such a double-layer structure that can exhibit well-controlled SW reflection-phase profiles by varying the permittivity distribution of the dielectric layer and place it on a plasmonic metal to efficiently control the wave fronts of SWs. As a proof of concept, we experimentally demonstrate in the microwave regime that our fabricated “metawall” can anomalously reflect SWs following the generalized Snell’s law. The working efficiency is about 70% at frequencies around 12 GHz. Among many possible applications, we finally employ full-wave simulations to demonstrate a SPP focusing effect at telecom wavelength, showing the robustness of our proposed strategy.

II. RESULTS AND DISCUSSION

A. Physical concept and model demonstration

We start by introducing the basic concept. Previous studies have shown that metasurfaces can modulate the wave fronts of PWs at will, achieving interesting physical effects such as anomalous reflection or light focusing depending on the phase distributions realized on the

metasurfaces, as schematically shown in Figs. 1(a) and 1(b). The basic idea is to use a carefully designed metasurface to locally control the phases of the impinging waves, thus, reshaping the wave fronts of reflected or refracted beams based on interferences. Inspired by this observation, here we propose to extend the idea of the metasurface to control the wave fronts of SWs. As shown in Figs. 1(c) and 1(d), we can put a carefully designed ultrathin metastructure (called a metawall) vertically on a plasmonic surface, which can also locally control the phase of an impinging SW. When a SW beam is launched on the plasmonic surface and strikes the metawall, the incident SW may gain different local phases from the reflections on the metawall, thus, generating a reflected SW beam with the desired wave front. By carefully designing metawalls exhibiting linear or parabolic reflection-phase profiles for SWs, we can realize anomalous reflection and focusing for a SW [see Figs. 1(c) and 1(d)].

We next describe how to design our metawalls. We find that a double-layer metastructure constructed by an ultrathin gradient-index dielectric layer and a metallic mirror can do the job. Specifically, the metallic mirror inside the structure ensures that the metawall can (nearly) totally reflect the SW wave, while the permittivity of the dielectric layer can be “tuned” to generate the appropriate local reflection phase ϕ . In principle, if the variation range of ϕ can cover 360° via tuning the refraction index of the dielectric layer, we can design metawalls exhibiting appropriate $\phi(y)$ profiles to efficiently reshape the SW wave fronts as desired. Specifically, if the phase profile of the metawall satisfies

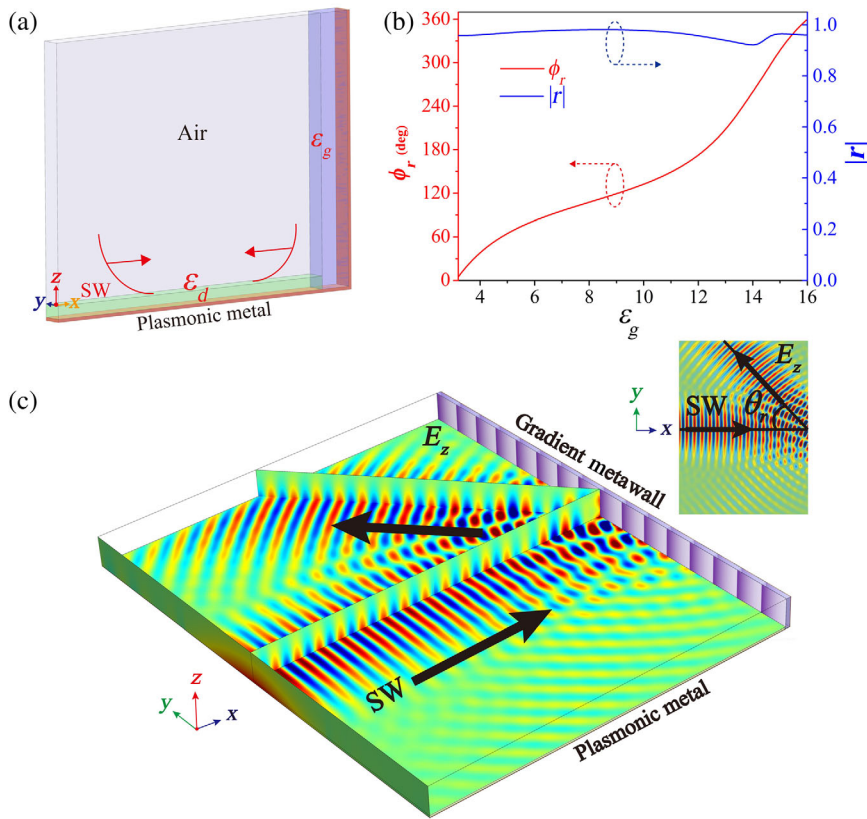


FIG. 2. Demonstration of the concept based on the model systems. (a) Simulation setup to obtain the SW reflection coefficient of the proposed metawall, which is composed of a 5-mm-thick dielectric slab (with permittivity ϵ_g) and a PEC mirror. (b) SW reflection amplitude and phase as functions of ϵ_g for the metawall depicted in (a) obtained by FEM simulations. (c) FEM-simulated near-field E_z pattern on a plane above the plasmonic metal, assuming that a SW Gaussian beam strikes the metawall. Here, the distribution of ϵ_g is such that the metawall exhibits a phase distribution satisfying Eq. (1) with $\xi = 0.75k_{\text{SW}}$. The working frequency is 12 GHz.

$$\phi(y) = \phi_0 + \xi y \quad (1)$$

for a SW at a particular frequency, the reflections of the SW by the metawall must be governed by the generalized Snell's law:

$$\sin \theta_r = \sin \theta_i + \frac{\xi}{k_{\text{SW}}}, \quad (2)$$

where θ_i and θ_r are the incident and reflective angles of the SW, respectively, k_{SW} is the wave vector of the SW at the working frequency, and ξ is the phase gradient provided by the metawall. On the other hand, we can use a metawall to focus the SW if the ϕ distribution of the metawall exhibits the following parabolic distribution:

$$\phi(y) = \phi_0 + k_{\text{SW}} \left(\sqrt{y^2 + F^2} - F \right), \quad (3)$$

where F denotes the focal length.

We perform numerical studies of effective-medium models to demonstrate that the idea indeed works. Without loss of generality, we choose the microwave regime to work in. Since natural SPPs do not exist in this frequency domain, we purposely adopt an artificial plasmonic structure, a perfect metallic conductor (PEC) ground plane covered by a 2-mm-thick dielectric spacer ($\epsilon_d = 2.65$) that can support guided SWs with a

well-defined dispersion relation working in the microwave regime [42–44] (see the Supplemental Material [45]). We next put a 32-mm-high *homogeneous* metawall vertically on the plasmonic structure and employ finite element method (FEM) simulations to calculate the reflection coefficient of SWs flowing on the plasmonic structure [see Fig. 2(a)]. The metawall consists of a 5-mm-thick dielectric layer (with permittivity ϵ_g) and a PEC mirror. In our calculations, we excite an eigen SW mode at the left boundary of the plasmonic structure using a surface current source and then study the stabilized EM field distributions inside the system. Finally, we numerically retrieve the SW reflection coefficient (including its amplitude and phase) by decomposing the simulated total fields to the incident and reflected SW signals. We set the frequency as 12 GHz at which the wave vector of the SW mode is $k_{\text{SW}} = 1.055k_0$ (with k_0 being the free-space wave vector), and we numerically compute the SW reflection coefficient as a function of ϵ_g and depict the results in Fig. 2(b). It is clear that the reflection phase of the metawall ϕ_r can cover the full range of 360° as we vary ϵ_g from 3 to 16. On the other hand, the SW reflection amplitude remains at around 0.9, indicating that the scatterings to the PWs are weak in such cases. The inherent working principle of our metawall is that it can couple the SW mode into a squeezed evanescent mode with a larger wave vector yet generate enough accumulated phase after reflection (see the Supplemental Material [45]).

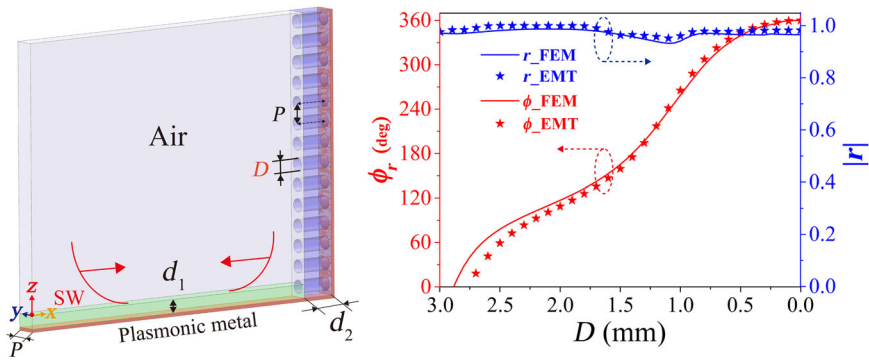


FIG. 3. SW reflection properties of the designed metawall. (a) Simulation setup to obtain the SW reflection coefficient of a nongradient metawall composed of a 5-mm-thick high-index slab ($\epsilon_d = 16$) drilled with subwavelength-scale airholes and a PEC mirror. By tuning the diameter D of the airholes, the effective permittivity of the whole dielectric layer can be freely tuned to mimic the model system depicted in Fig. 2(a). (b) FEM-simulated reflection amplitude and phase versus the diameter D based on the practical structure (line) and the retrieved effective-medium model (star). Here, the frequency is fixed at 12 GHz.

Based on the numerical results shown in Fig. 2(b), we can design a gradient-index metawall with an appropriate $\epsilon_d(y)$ profile such that the $\phi(y)$ distribution of the whole device satisfies Eq. (1) with $\xi = 0.75k_{SW}$. Putting the designed metawall vertically on the artificial plasmonic surface, we perform FEM simulations to study the reflections of the SWs. Figure 2(c) depicts the calculated E_z field pattern on the artificial plasmonic structure with an efficiency of about 80%. Here, we numerically integrate out the power carried by the anomalously reflected SW beam and then evaluate the working efficiency of the SW anomalous reflection by calculating the ratio between it and that of the incident SW beam. Different from conventional metasurfaces for controlling PWs, the proposed metawall for the SWs will inevitably suffer from scattering losses, leading to efficiency less than 1. In the present case, the scattering loss of our device is less than 10%.

B. Design and fabrication of metawalls for SW anomalous reflection

We now move on to design a realistic metawall in the microwave regime. Obviously, the key challenge is to find dielectric materials with permittivity varying in a large-enough range [see Fig. 2(b)]. Inspired by other practical realizations of dielectric metasurfaces [31,46,47], we adopt a high-index ($\epsilon_d = 16$) slab drilled with subwavelength-scaled airholes to mimic a “homogeneous” dielectric material with certain permittivity. Figure 3(a) shows the schematic of a designed metawall where the airholes (with diameters D) are arranged in a two-dimensional square lattice with periodicity $P = 3$ mm. Based on the effective-medium theory (EMT), we can “tune” the value of D to achieve a desired (*effective*) permittivity of the whole dielectric slab and, in turn, a desired reflection phase ϕ for the SW. We employ full-wave simulations to demonstrate this point based on the same configuration and calculation technique as in Fig. 2(a). Figure 3(b) shows that at a frequency of 12 GHz, the SW reflection phase of such metawalls can indeed cover the full range of 360° if we vary the parameter D from 0 to 2.88 mm. Meanwhile,

SW reflection amplitude is also kept at a high value (larger than 0.9) in the whole spectrum. To understand the physics more deeply, we employ EMT to retrieve the effective permittivity tensor of such a complex medium [48–50] noting that all characteristic inhomogeneity length scales (i.e., P , D) are much smaller than the EM wavelength (25 mm). The results obtained based on the EMT-retrieved parameters are in excellent agreement with the full-wave-simulation results based on practical structures [see Fig. 3(b) and the Supplemental Material [45]], indicating that the working mechanism of our metawall is essentially the same as that in Fig. 2(a).

Based on the results presented in Fig. 3, we next design and fabricate a gradient metawall (with $\xi = 0.79k_{SW}$ at $f = 12$ GHz) and experimentally demonstrate its capabilities to control the wave front of the SW on the designed artificial plasmonic metal. Figure 4(a) depicts part of the picture of the fabricated sample. A supercell of the fabricated gradient metawall consists of ten lines of airholes with diameters varying from 0 to 2.77 mm, yielding a linear phase change of ϕ based on the results shown in Fig. 3(b). According to Eq. (2), the anomalous reflection angle for the SW is predicted as 52.2° at normal incidence. We first employ FEM simulations to calculate the E_z field pattern generated on the system as a Gaussian SW beam is launched on the plasmonic surface and strikes normally on the metawall. As shown in Fig. 4(b), the SW beam reflected by the metawall does flow along a nonspecular direction at $\theta_r \approx 52.3^\circ$, matching well with the theoretical prediction. We note that both the specular reflection and -1 -order diffraction are deeply suppressed, already implying a high efficiency of the anomalous reflection. The working efficiency, thus evaluated is 70%, where the missing powers are carried out by the scatterings to the far field as PWs (approximately 13%), normal reflection (about 9%), and -1 -order diffraction of SWs (about 7%). The performance of our metawall can be further improved by carefully optimizing the design (e.g., using higher-index material, thinner thickness, or more unit cells inside the metawall).

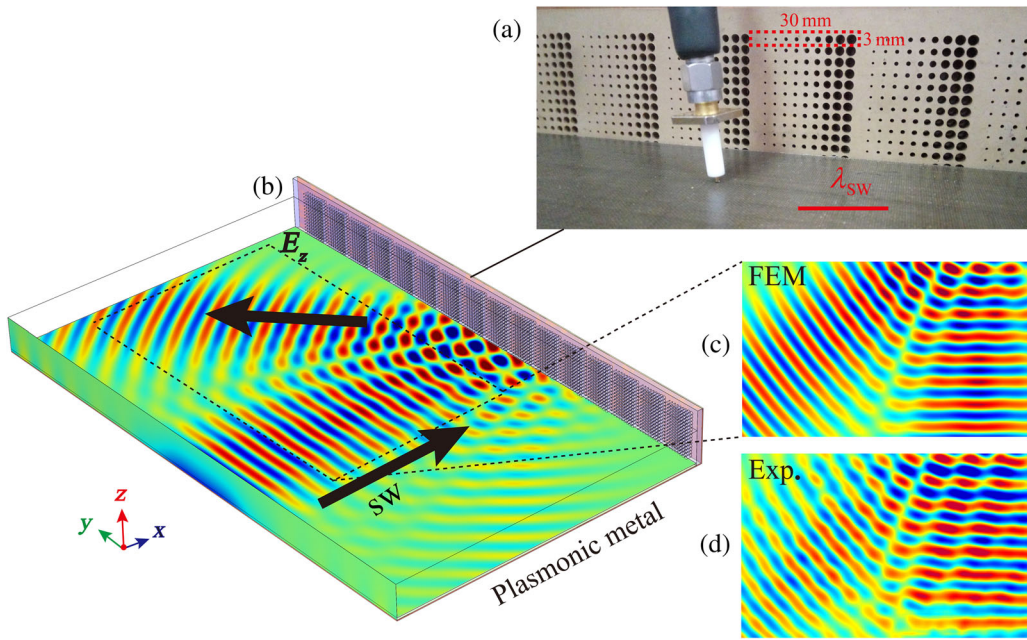


FIG. 4. Near-field characterizations of the anomalous reflection phenomenon for a SW. (a) Part of the picture showing the experimental setup, including the metawall, plasmonic metal, and a detecting monopole antenna. Here, one supercell of the metawall consists of ten unit cells with the diameters of the airholes changing from 0 to 2.77 mm. (b) FEM-simulated near-field E_z pattern on a plane 2 mm above the plasmonic metal, where a launched SW wave strikes the metawall. In the measurement, a monopole antenna is used to probe the SW field distribution (E_z) above the plasmonic metal, with $(300 \times 200 \text{ mm}^2)$ -sized images obtained by near-field scanning measurements (d). As a comparison, FEM simulation with the same length scale is reproduced in (c). Here, the working frequency is 12 GHz.

We note that the process of designing metawalls for SW manipulation is similar to that of designing metawalls for PW manipulations. The most essential difference is that a metawall inevitably suffers from the scattering losses to the far field, and, thus, one has to carefully optimize the structure in the design process. However, the vertical size of a metawall does not need to be very large (as long as it is larger than the decay length of the considered SW), which is an obvious advantage as compared with the metasurface design for PW manipulations.

We finally demonstrate such anomalous SW reflection by microwave experiments. The whole experimental setup consists of an artificial plasmonic metal and a metawall, as shown in Fig. 4(a). In our experiments, we first excite a SW beam on the artificial plasmonic metal employing a SW metacoupler proposed in Ref. [24] (see the Supplemental Material [45]). The excited SW then propagates on the artificial plasmonic metal and is reflected anomalously when it strikes the metawall. A monopole antenna is moved on a plane 2 mm above the plasmonic metal to measure the E_z field distribution. Both the monopole antenna and excited horn are connected to a vector network analyzer (Agilent E8362CPNA) so that the near-field-measured E_z field can contain both amplitude and phase information. Figure 4(d) shows the measured near-field E_z distribution on the plasmonic metal. Restricted by our experimental setup, we scan only an area of $300 \times 200 \text{ mm}^2$, which is

enough to demonstrate the anomalous reflection effect [see Fig. 4(d)]. The measured results are in good agreement with the corresponding FEM simulations inside the same area [see Fig. 4(c)]. From the measured E_z pattern, we can clearly identify that the anomalous reflection angle is $\theta_r \approx 51^\circ$ [see Fig. 4(d)], again matching well with the theoretical prediction (i.e., 52.2°). Furthermore, the parallel wave vector of the anomalously reflected beam depicted in Fig. 4(d) is measured to be $k_{SW} \approx 1.042k_0$, agreeing well with the value $k_{SW} = 1.055k_0$ predicted theoretically for this frequency and reinforcing our claim that the reflected signals are indeed from reflected SWs. This evidence undoubtedly demonstrates the desired SW-manipulation functionality of the designed metawall. Unfortunately, it is very difficult to experimentally retrieve the efficiency of SW anomalous reflection via the power-flow-integration technique. However, we can still see a reasonably high efficiency since the measured field amplitudes of the incident and anomalous reflected SW beams are comparable [see Figs. 4(c) and 4(d)]. In our experimental setup, the incident angle of the launched SW is fixed by a metacoupler, which is difficult to change, and, therefore, we cannot verify the generalized Snell's law for the SW anomalous reflection experimentally. Rather, we adopt FEM simulations to demonstrate this point, where the anomalous negative reflection effect can also happen in certain cases (see the Supplemental Material [45]).

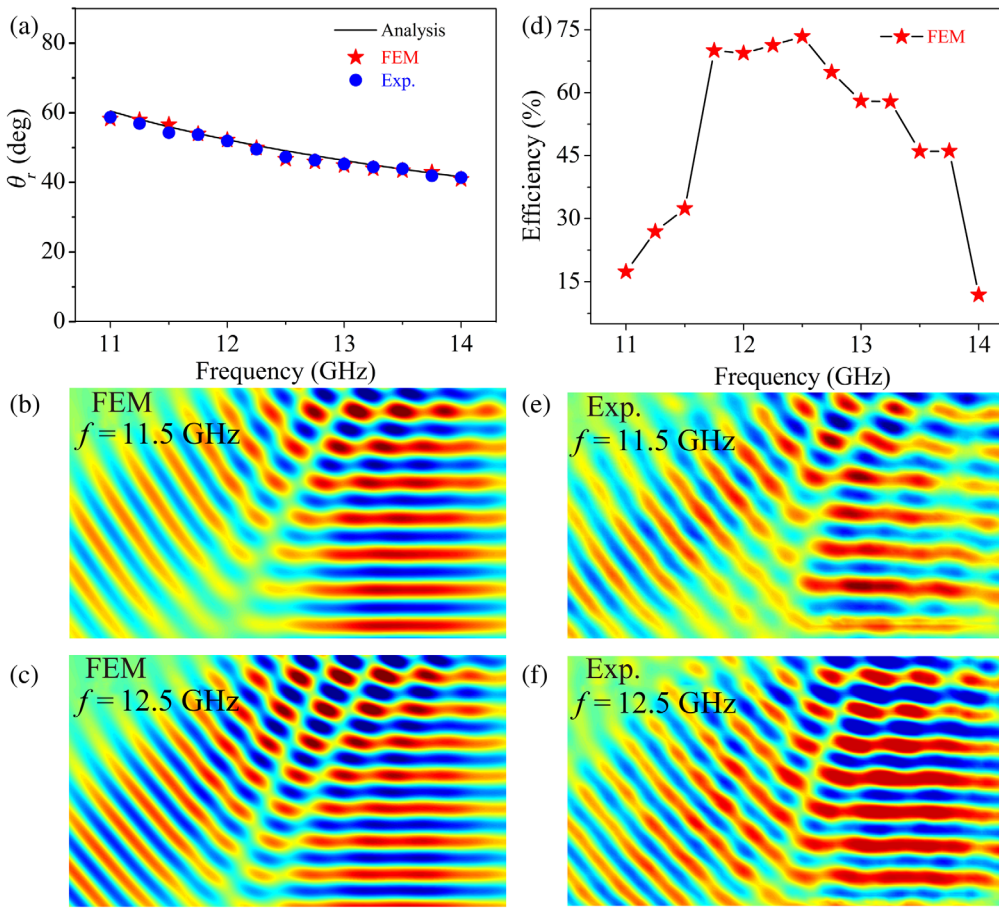


FIG. 5. Verification of the anomalous reflection effect for a SW within a frequency band. (a) The measured anomalous reflection angle θ_r as the function of the working frequency obtained via FEM simulations (star), near-field experiments (dot), and theoretical analysis Eq. (2) (line). The E_z field patterns on the plasmonic metal obtained by FEM simulations (b),(c) and experiments (e),(f) at 11.5 GHz (b),(e), and 12.5 GHz (c),(f). (d) The retrieved efficiencies of the anomalous reflection versus frequency via FEM simulations.

Such an anomalous SW reflection effect can exist within a certain frequency band. Figures 5(b) and 5(c) show the measured E_z field patterns at two representative frequencies (11.5 and 12.5 GHz), which match well with the corresponding FEM simulations [Figs. 5(e) and 5(f)]. Based on the measured and simulated results within the frequency band 11–14 GHz, we obtain how the reflection angle θ_r varies against the frequency and then depict the relationships in Fig. 5(a). We find that both FEM simulations (stars) and experiments (circles) are in perfect agreement with the theoretical prediction of Eq. (2) (solid line) assuming that ξ is a frequency-independent constant. This is side evidence demonstrating that our anomalous SW reflection is indeed governed by the generalized Snell's law. Moreover, we also perform FEM simulations to calculate the working efficiencies of the SW anomalous reflection within this band. Figure 5(d) shows that our designed metawall possesses a SW anomalous reflection efficiency higher than 0.5 within (11.75–12.75 GHz), yielding a bandwidth of 1 GHz. Outside this frequency band, the working efficiency drops significantly since the resultant SW reflection phase profile gradually deviates from Eq. (1), leading to stronger scatterings to normal and -1-order diffraction modes.

C. Extensions to high frequencies

The strategy proposed in this paper is so general that one can also employ it to realize SPP wave-front control in higher-frequency domains. As an illustration, we design a metawall to realize the SPP focusing effect at telecom wavelength. Figure 6(a) shows the schematic setup of the SPP metalens with a focal length of $8 \mu\text{m}$ and a numerical aperture (NA) of 0.8. In our design, the metawall is $3 \mu\text{m}$ high and is composed of a 450-nm-thick silicon ($\epsilon_{\text{Si}} = 12.1$) layer drilled with inhomogeneous airhole arrays and a 200-nm-thick Au film. The lattice constant of the airhole array is 300 nm, while the airhole diameters vary from 0 to 276 nm. As shown in Fig. 6(b), the plasmonic surface is constructed by capping 100-nm SiO_2 on a flat Au film. The SiO_2 film is adopted to increase the mode index of hybrid SPP on the Au surface [25]. Figure 6(c) depicts the simulated near-field distribution at a plane 10 nm above the plasmonic metal when a SPP beam is launched on its surface and reflected back by the metawall. Clearly, the reflected SPP waves converge to a focal point at the desired position, demonstrating our theoretical prediction. Figure 6(d) shows the field intensity distribution of the focused SPP at the focal line marked as the blue dashed line in Fig. 6(c). The peak width is about

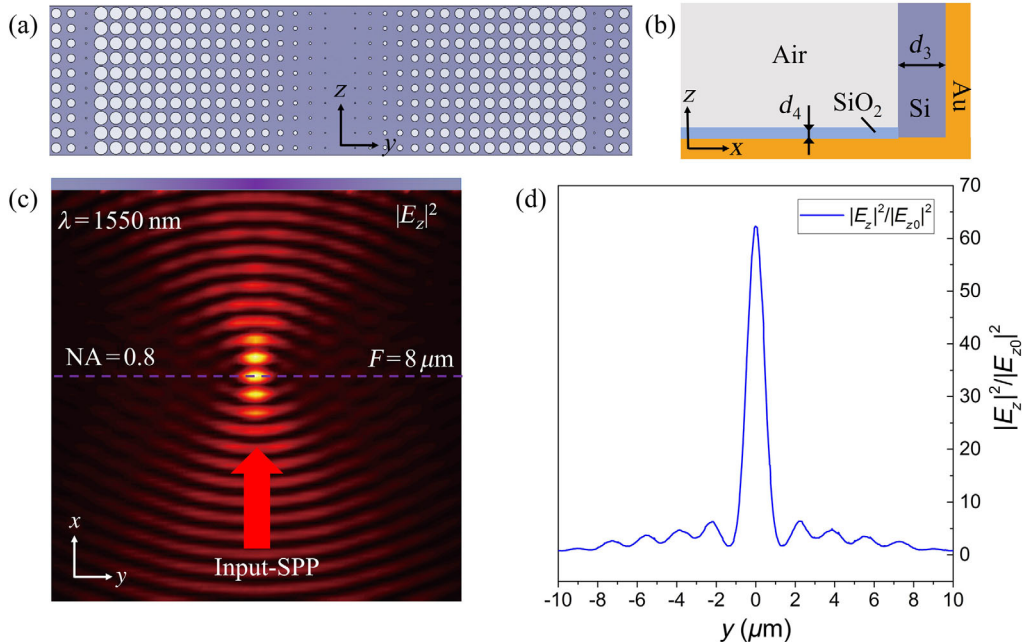


FIG. 6. Demonstration of the SPP focusing effect at telecom wavelength. (a) The top view of the designed metasurface composed of 450-nm-thick (d_3) silicon filled with an inhomogeneous airhole array and an Au film. The lattice constant is 300 nm, and the diameters of the airholes vary from 0 to 276 nm. (b) The side view of the plasmonic metal and the metasurface. Here, the plasmonic metal is designed by capping 100-nm-thick (d_4) SiO₂ on a flat Au film. (c) FEM-simulated near-field distribution above the plasmonic metal under the illumination of a SPP Gaussian beam along the x direction. Here, E_{z0} denotes the field amplitude at the center of the incident SPP Gaussian beam, the wavelength is 1550 nm, and the focal length is demonstrated as $8 \mu\text{m}$. (d) The near-field distribution of SPP at the focal length position versus the y coordinate.

1038 nm, which is close to the diffraction limit described by the equation $d = \lambda/(2 \times \text{NA}) \approx 969 \text{ nm}$.

III. CONCLUSION

To summarize, we successfully extend the concept of wave-front manipulation with a metasurface from the far field to the near field. The proposed metawall composed of a subwavelength-thick gradient-index dielectric layer and a flat metallic mirror can (nearly) totally reflect a SW with desired phase modulation, and, thus, it can efficiently control the SW wave fronts. We perform both numerical simulations and proof-of-concept microwave experiments to demonstrate this idea, showing that the SW can be anomalously reflected following a generalized Snell's law with about 70% efficiency within a broad frequency band. Such a scheme can also be extended to higher frequencies, and we employ full-wave simulations to demonstrate a SPP metasurface working at the wavelength of 1550 nm and exhibiting a focal length of $8 \mu\text{m}$. Our findings can stimulate many practical applications, such as SW holograms, complex SW beam generation, super-resolution imaging, enhanced nonlinear effects, and so on.

ACKNOWLEDGMENTS

This work is supported by the National Natural Science Foundation of China (Grants No. 11404063,

No. 11474057, No. 11774064, No. 11734007, and No. 11674068), the National Basic Research Program of China (Grant No. 2017YFA0303500), the Shanghai Science and Technology Committee (Grants No. 16ZR1445200 and No. 16JC1403100), the Changchun Institute of Optics, Fine Mechanics and Physics, Chinese Academy of Sciences, the National University Student Innovation Program (No. 201510246084), and the Hui-Chun Chin and Tsung-Dao Lee Chinese Undergraduate Research Endowment No. 15031.

- [1] W. L. Barnes, A. Dereux, and T. W. Ebbesen, Surface plasmon subwavelength optics, *Nature (London)* **424**, 824 (2003).
- [2] N. Fang, H. Lee, C. Sun, and X. Zhang, Sub-diffraction-limited optical imaging with a silver superlens, *Science* **308**, 534 (2005).
- [3] D. K. Gramotnev and S. I. Bozhevolnyi, Plasmonics beyond the diffraction limit, *Nat. Photonics* **4**, 83 (2010).
- [4] J. N. Anker, W. P. Hall, O. Lyandres, N. C. Shah, J. Zhao, and R. P. Van Duyne, Biosensing with plasmonic nanosensors, *Nat. Mater.* **7**, 442 (2008).
- [5] R. Zia, J. A. Schuller, A. Chandran, and M. L. Brongersma, Plasmonics: The next chip-scale technology, *Mater. Today* **9**, 20 (2006).

- [6] A. Hohenau, J. R. Krenn, A. L. Stepanov, A. Drezet, H. Ditlbacher, B. Steinberger, A. Leitner, and F. R. Aussenegg, Dielectric optical elements for surface plasmons, *Opt. Lett.* **30**, 893 (2005).
- [7] E. Devaux, J.-Y. Laluet, B. Stein, C. Genet, T. Ebbesen, J.-C. Weeber, and A. Dereux, Refractive micro-optical elements for surface plasmons: From classical to gradient index optics, *Opt. Express* **18**, 20610 (2010).
- [8] H. Ditlbacher, J. R. Krenn, G. Schider, A. Leitner, and F. R. Aussenegg, Two-dimensional optics with surface plasmon polaritons, *Appl. Phys. Lett.* **81**, 1762 (2002).
- [9] I. P. Radko, A. B. Evlyukhin, A. Boltasseva, and S. I. Bozhevolnyi, Refracting surface plasmon polaritons with nanoparticle arrays, *Opt. Express* **16**, 3924 (2008).
- [10] S. Randhawa, M. U. González, J. Renger, S. Enoch, and R. Quidant, Design and properties of dielectric surface plasmon Bragg mirrors, *Opt. Express* **18**, 14496 (2010).
- [11] A. Minovich, A. E. Klein, N. Janunts, T. Pertsch, D. N. Neshev, and Y. S. Kivshar, Generation and Near-Field Imaging of Airy Surface Plasmons, *Phys. Rev. Lett.* **107**, 116802 (2011).
- [12] L. Li, T. Li, S. M. Wang, C. Zhang, and S. N. Zhu, Plasmonic Airy Beam Generated by In-Plane Diffraction, *Phys. Rev. Lett.* **107**, 126804 (2011).
- [13] A. Drezet, A. L. Stepanov, H. Ditlbacher, A. Hohenau, B. Steinberger, F. R. Aussenegg, A. Leitner, and J. R. Krenn, Surface plasmon propagation in an elliptical corral, *Appl. Phys. Lett.* **86**, 074104 (2005).
- [14] L. Li, T. Li, S. Wang, S. Zhu, and X. Zhang, Broad band focusing and demultiplexing of in-plane propagating surface plasmons, *Nano Lett.* **11**, 4357 (2011).
- [15] L. Li, T. Li, S. M. Wang, and S. N. Zhu, Collimated Plasmon Beam: Nondiffracting versus Linearly Focused, *Phys. Rev. Lett.* **110**, 046807 (2013).
- [16] Y.-G. Chen, Y.-H. Chen, and Z.-Y. Li, Direct method to control surface plasmon polaritons on metal surfaces, *Opt. Lett.* **39**, 339 (2014).
- [17] Y. G. Chen and Z. Y. Li, Three-dimensional manipulations of surface plasmon polariton wave propagation, *Plasmonics* **11**, 1385 (2016).
- [18] Y. Liu, T. Zentgraf, G. Bartal, and X. Zhang, Transformational plasmon optics, *Nano Lett.* **10**, 1991 (2010).
- [19] P. a Huidobro, M. L. Nesterov, L. Martín-Moreno, and F. J. García-Vidal, Transformation optics for plasmonics, *Nano Lett.* **10**, 1985 (2010).
- [20] A. Vakil and N. Engheta, Transformation optics using graphene, *Science* **332**, 1291 (2011).
- [21] N. Yu, P. Genevet, M. a. Kats, F. Aieta, J.-P. Tetienne, F. Capasso, and Z. Gaburro, Light propagation with phase discontinuities: Generalized laws of reflection and refraction, *Science* **334**, 333 (2011).
- [22] X. Ni, N. K. Emani, A. V. Kildishev, A. Boltasseva, and V. M. Shalaev, Broadband light bending with plasmonic nanoantennas, *Science* **335**, 427 (2012).
- [23] S. Sun, K. Yang, C. Wang, T. Juan, W. T. Chen, C. Y. Liao, Q. He, S. Xiao, W. Kung, G. Guo, L. Zhou, and D. P. Tsai, High-efficiency broadband anomalous reflection by gradient meta-surfaces, *Nano Lett.* **12**, 6223 (2012).
- [24] S. Sun, Q. He, S. Xiao, Q. Xu, X. Li, and L. Zhou, Gradient-index meta-surfaces as a bridge linking propagating waves and surface waves, *Nat. Mater.* **11**, 426 (2012).
- [25] A. Pors, M. G. Nielsen, T. Bernardin, J.-C. Weeber, and S. I. Bozhevolnyi, Efficient unidirectional polarization-controlled excitation of surface plasmon polaritons, *Light Sci. Appl.* **3**, e197 (2014).
- [26] J. Lin, J. P. B. Mueller, Q. Wang, G. Yuan, N. Antoniou, X.-C. Yuan, and F. Capasso, Polarization-controlled tunable directional coupling of surface plasmon polaritons, *Science* **340**, 331 (2013).
- [27] L. Huang, X. Chen, B. Bai, Q. Tan, G. Jin, T. Zentgraf, and S. Zhang, Helicity dependent directional surface plasmon polariton excitation using a metasurface with interfacial phase discontinuity, *Light Sci. Appl.* **2**, e70 (2013).
- [28] W. Sun, Q. He, S. Sun, and L. Zhou, High-efficiency surface plasmon meta-couplers: Concept and microwave-regime realizations, *Light Sci. Appl.* **5**, e16003 (2016).
- [29] X. Li, S. Xiao, B. Cai, Q. He, T. J. Cui, and L. Zhou, Flat metasurfaces to focus electromagnetic waves in reflection geometry, *Opt. Lett.* **37**, 4940 (2012).
- [30] X. Chen, L. Huang, H. Muhlenbernd, G. Li, B. Bai, Q. Tan, G. Jin, C.-W. W. Qiu, T. Zentgraf, and S. Zhang, Reversible three-dimensional focusing of visible light with ultrathin plasmonic flat lens, *Adv. Opt. Mater.* **1**, 517 (2013).
- [31] M. Khorasaninejad, W. T. Chen, R. C. Devlin, J. Oh, A. Y. Zhu, and F. Capasso, Metalenses at visible wavelengths: Diffraction-limited focusing and subwavelength resolution imaging, *Science* **352**, 1190 (2016).
- [32] S. Wang, P. C. Wu, V.-C. Su, Y.-C. Lai, C. Hung Chu, J.-W. Chen, S.-H. Lu, J. Chen, B. Xu, C.-H. Kuan, T. Li, S. Zhu, and D. P. Tsai, Broadband achromatic optical metasurface devices, *Nat. Commun.* **8**, 187 (2017).
- [33] C. Pfeiffer and A. Grbic, Metamaterial Huygens' Surfaces: Tailoring Wave Fronts with Reflectionless Sheets, *Phys. Rev. Lett.* **110**, 197401 (2013).
- [34] C. Pfeiffer and A. Grbic, Controlling Vector Bessel Beams with Metasurfaces, *Phys. Rev. Applied* **2**, 044012 (2014).
- [35] E. Karimi, S. A. Schulz, and I. De Leon, Generating optical orbital angular momentum at visible wavelengths using a plasmonic metasurface, *Light Sci. Appl.* **3**, e167 (2014).
- [36] W. T. Chen, K. Yang, C. Wang, Y. Huang, G. Sun, C. Y. Liao, W. Hsu, H. T. Lin, S. Sun, L. Zhou, A. Q. Liu, and D. P. Tsai, High-efficiency broadband meta-hologram with polarization-controlled dual images, *Nano Lett.* **14**, 225 (2014).
- [37] G. Zheng, H. Mühlenbernd, M. Kenney, G. Li, T. Zentgraf, and S. Zhang, Metasurface holograms reaching 80% efficiency, *Nat. Nanotechnol.* **10**, 308 (2015).
- [38] X. Ni, A. V. Kildishev, and V. M. Shalaev, Metasurface holograms for visible light, *Nat. Commun.* **4**, 2807 (2013).
- [39] H. Mühlenbernd, P. Georgi, N. Pholchai, L. Huang, G. Li, S. Zhang, and T. Zentgraf, *ACS Photonics* **3**, 124 (2016).
- [40] M. Papaioannou, E. Plum, J. Valente, E. Rogers, and Nikolay I. Zheludev, *Light Sci. Appl.* **5**, e16070 (2016).
- [41] Z. H. Wang, S. C. Jiang, X. Xiong, R. W. Peng, and M. Wang, *Appl. Phys. Lett.* **108**, 261107 (2016).
- [42] J. B. Pendry, L. Martín-Moreno, and F. J. Garcia-Vidal, Mimicking surface plasmons with structured surfaces, *Science* **305**, 847 (2004).

- [43] F. J. García-Vidal, L. Martín-Moreno, and J. B. Pendry, Surfaces with holes in them: New plasmonic metamaterials, *J. Opt. A* **7**, S97 (2005).
- [44] L. Zhou and C. T. Chan, High-impedance reflectivity and surface-wave band gaps in metamaterials, *Appl. Phys. Lett.* **84**, 1444 (2004).
- [45] See Supplemental Material at <http://link.aps.org/supplemental/10.1103/PhysRevApplied.9.014032> for the dispersion relation of eigen SW on the artificial plasmonic structure, mechanism of SW phase modulation with the proposed metawall, effective-medium property of the practical metawall shown in Fig. 3(a), details of the SW metacoupler utilized in microwave experiments, and incidence-angle dependence of the SW anomalous reflection effect.
- [46] S. Jiang, X. Xiong, Y. Hu, S. Jiang, Y. Hu, D. Xu, R. Peng, and M. Wang, High-efficiency generation of circularly polarized light via symmetry-induced anomalous reflection, *Phys. Rev. B* **91**, 125421 (2015).
- [47] M. Decker, High-efficiency dielectric Huygens' surfaces, *Adv. Opt. Mater.* **3**, 813 (2015).
- [48] D. A. G. Bruggeman, Berechnung verschiedener physikalischer Konstanten von heterogenen Substanzen. I. Dielektrizitätskonstanten und Leitfähigkeiten der Mischkörper aus isotropen Substanzen, *Ann. Phys. (Berlin)* **416**, 636 (1935).
- [49] S. M. Rytov, Electromagnetic properties of a finely stratified medium, *Sov. Phys. JETP* **2**, 466 (1956).
- [50] S. Sun, X. Huang, and L. Zhou, Two-dimensional complete photonic gaps from layered periodic structures containing anisotropic left-handed metamaterials, *Phys. Rev. E* **75**, 066602 (2007).